A passively safe and gravity-counterbalanced anthropomorphic robot arm

John P. Whitney[1] and Jessica K. Hodgins[2]

Abstract— When designing a robot for human-safety during direct physical interaction, one approach is to size the robot's actuators to be physically incapable of exerting damaging impulses, even during a controller failure. Merely lifting the arms against their own weight may consume the entire available torque budget, preventing the rapid and expressive movement required for anthropomorphic robots. To mitigate this problem, gravity-counterbalancing of the arms is a common tactic; however, most designs adopt a shoulder singularity configuration which, while favorable for simple counterbalance design, has a range of motion better suited for industrial robot arms. In this paper we present a shoulder design using a novel differential mechanism to counterbalance the arm while preserving an anthropomorphically favorable singularity configuration and natural range-of-motion. Furthermore, because the motors driving the shoulder are completely grounded, counterbalance masses or springs are easily placed away from the shoulder and low in the torso, improving mass distribution and balance. A robot arm using this design is constructed and evaluated for counterbalance efficacy and backdrivability under closed-loop force control.

I. INTRODUCTION

Robots are increasingly used outside the factory setting—in surgery, patient therapy, home service, entertainment, and many other applications [1]–[4]. A robot working in direct contact with humans must meet a high standard for safety, but it should also be designed—physically and functionally—to be compatible with the speed, dexterity, and range-of-motion of its human counterpart. This need is self-evident for rehabilitation, exoskeleton, and entertainment character robots, but anthropomorphic configurations are now used for factory robots as well [5].

In this paper, we consider only robots that are "passively safe", meaning the robot's actuators are physically incapable of moving the arms in any way that can cause injury to a human. Maximum limb speed is set by limb inertia, surface compliance, geometry, and the pressure and impulse limits specified by the relevant safety standard [6].

Excepting high-speed robot arms, gravity loads often dominate torque loads. For a passively safe design, overcoming gravity may consume all available torque, limiting the arm to low-speed operation. Gravity counterbalancing using either counterweights or springs allows motors to be sized to the dynamic loads, allowing for faster motion. A counterbalance allows for smaller motors, and resting power consumption

is greatly reduced, a benefit to mobile applications. Counterbalancing is no panacea; counterweights add significantly to arm mass—especially for compact configurations—and counterspring systems are mechanically complex.

In this paper, we introduce a counterbalance design that allows for an anthropomorphically favorable shoulder singularity using a differential mechanism. Through the differential, both axes are grounded in this design, allowing the motors and counterweights (or counterspring assemblies) to be remotely located, for better packaging and mass distribution. By reducing motor torque requirements, a small gear ratio can be used, allowing a backdriveable design appropriate for impedance-mediated interaction [7].

This work is inspired by many related efforts. The WAM arm [3] demonstrated backdrivable designs for compliant and natural human interaction. Others [1], [8], [9] use a counterbalance to maximize performance given human-safety constraints. Bringing counterbalance springs inside the arm [10], [11] and moving counterweights away from the arm can prevent counterbalance interference [12]. Our design seeks a combination of these characteristics: human-like range-of-motion, backdrivability, and remote actuation and counterbalancing.

II. GRAVITY COUNTERBALANCING

The advantages of counterbalancing a robot arm are evident from a simple dimensional analysis. Consider a single-link robot arm of length L, with constant cross-sectional area A, and uniform density ρ. When outstretched horizontally, the static moment due to gravity is maximal:

$$(\tau_{\text{stat}})_{\text{max}} = (\rho A L) g \frac{L}{2}. \tag{1}$$

Dynamic torque is highest at maximum acceleration, $(\tau_{\text{dyn}})_{\text{max}} = I \ddot{\phi}_{\text{max}}$, where I is the mass moment of inertia, $I = \frac{1}{3}(\rho A L)L^2$, and $\ddot{\phi}_{\text{max}}$ is the peak angular acceleration. Assuming point-to-point motion with a sinusoidal velocity profile, the acceleration is

$$\ddot{\phi} = \omega^2 \Phi \sin(\omega t), \tag{2}$$

where ω is the angular frequency, given by $\omega = \dot{\phi}_{\text{max}}/\Phi$, where Φ is the angle moved, and $\dot{\phi}_{\text{max}}$ is the peak angular velocity. Thus we find a peak angular acceleration $\ddot{\phi}_{\text{max}} = \dot{\phi}_{\text{max}}^2/\Phi$, and the ratio between peak static and dynamic torque for our robot arm is

$$\frac{(\tau_{\text{stat}})_{\text{max}}}{(\tau_{\text{dyn}})_{\text{max}}} = \frac{\frac{3}{2}g\Phi}{L\dot{\phi}_{\text{max}}^2}. \tag{3}$$

[1]John P. Whitney is with Disney Research, Pittsburgh, PA 15213, USA peter.whitney@disneyresearch.com

[2]Jessica K. Hodgins is with Disney Research and the Robotics Institute, Carnegie Mellon University; Pittsburgh, PA 15213, USA jkh@disneyresearch.com
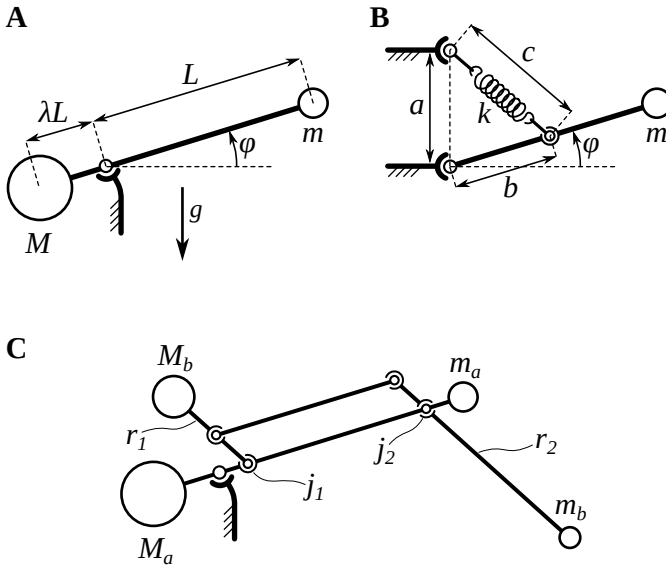
Fig. 1. Simple methods of mass- and spring-based gravity compensation for one- and two-link robot arms. A single link is trivially balanced with a single counterweight, (**A**). Balancing with a zero free-length spring, (**B**). When balancing serial links, a pantograph mechanism may be used to move distal link counterweights closer to the shoulder, (**C**).

Consider an arm 60 cm long, rotating through 180 degrees, reaching a peak velocity of 60 rpms (one revolution per second). According to Equation 3, peak static torques are then 1.9 times larger than dynamic torques. Slower peak velocities or shorter arms lead to even higher static loads. Consider as well the thermal nature of electric motors; without counterbalancing, they must be sized by their continuous rather than instantaneous torque rating. To maintain safety, motor torques must then be electronically limited at the amplifier to prevent the motor from applying torques above its continuous rating. With counterbalancing, the lower duty cycle of high-speed motion in many cases will allow the motors to be sized by their instantaneous torque rating, reducing motor mass by a factor of two or more.

A. Counterbalancing Techniques

Figure 1-A illustrates the simplest possible counterbalance design for a single link robot arm with a lumped mass m and length L. A single counterweight with mass $M = m/\lambda$ balances the arm for three degree-of-freedom (DOF) angular motion about the shoulder, where λ is the counterbalance moment arm as a fraction of L. To make the arm compact, and prevent interference with the body, we require small λ— say $\lambda \leq 0.2$—but this will increase the mass of the arm by a factor of six or more. Fortunately, total inertia scales as $I/(mL^2) = 1 + \lambda$, so compact counterbalance configurations increase rotational inertia only slightly.

Springs are more mass efficient at storing potential energy; Figure 1-B illustrates an equivalent spring-based balancing method. A spring is attached to the arm at a distance b from the shoulder and grounded at a height a, directly above the shoulder. Via the Pythagorean theorem, we obtain the length

of the spring, c, as a function of the arm's angle above horizontal, ϕ,

$$c^2 = a^2 + b^2 - 2ab \sin \phi. \tag{4}$$

We then obtain the total potential energy of the mass and spring,

$$U = mgL \sin \phi + \frac{1}{2}k(a^2 + b^2 - 2ab \sin \phi), \tag{5}$$

where k is the spring constant, and the spring is a so-called "zero free-length spring", i.e. it has a restoring force of $-kx$, where x is the absolute displacement/length of the spring. We see that if

$$mgL = kab, \tag{6}$$

then the potential energy is constant for any configuration of the arm. Springs can be made zero free-length, with difficulty, by winding them with a pre-stress. A zero free-length equivalent system is also achieved with a normal spring, cable, and idler pulley, arranged as described in [13].

Balanced links can be serially connected, but arm mass rises exponentially with the number of links, as each must balance the mass *and* counterweight mass of all downstream links. Figure 1-C shows how a pantograph parallel mechanism can be employed to move the forearm counterweight towards the shoulder. The orientation of forearm link r_2 is reflected by pantograph link r_1. If joint j_1 is moved to coincide with the shoulder center, then M_a and M_b can be replaced with countersprings [1], [8], [9]. Instead of coupling the forearm position back to the shoulder via pantograph, an alternative method is to bring a reference of the vertical orientation out to the elbow [10]. In [11], bevel gears are employed to also bring counterbalance springs for the upper arm into the arm as well, increasing the available range of motion.

B. Shoulder Configurations

Neglecting scapular motion [14], the human arm consists of a ball-joint shoulder (3DOF) and a revolute joint elbow (1DOF), as shown in Figure 2-A. An RRR configuration is commonly used to approximate the ball-joint. Configuration B is used in the PR-1 and Baxter quasi-anthropomorphic service and industrial robots [1], [5]. A convenience of this configuration is that the grounded shoulder joint j_1 is aligned with the direction of gravity, and a counterbalance spring can be connected between j_1 and j_3. This "flying" spring stays in a fixed plane that rotates with j_1, and therefore does not need universal joint connections at either end. However, this configuration is singular when the upper arm hangs straight down, a common pose for a human.

Configuration C removes this unfavorable singularity, but now a counterbalance spring must be attached to the upper arm with a universal joint. In this configuration, when the second joint "abducts" to 90 degrees, the shoulder becomes singular for upper arm rotation, which lacks a dedicated joint.

Configuration D, where j_1 points laterally, is very common for humanoid robots designed to mimic human motion [2], [15]. The upper arm is singular when aligned with j_1;
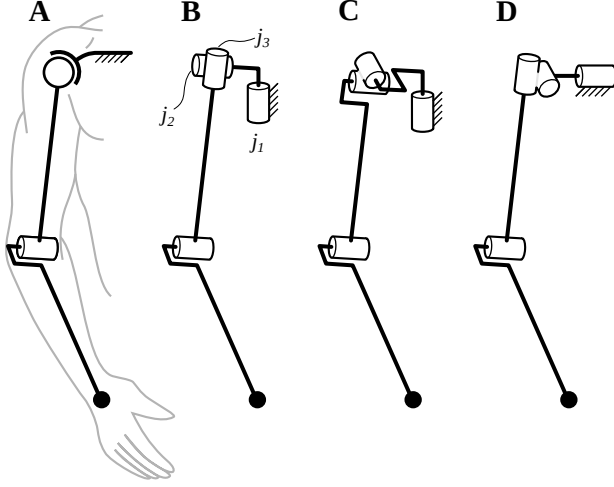
Fig. 2. Neglecting scapular motion, human arm kinematics are well approximated by a ball-and-socket joint at the shoulder (singularity-free) and a rotary joint at the elbow (**A**). Three approximations to this configuration are shown (**B-D**), with the ball-and-socket joint replaced by a three-joint assembly. Starting from ground, the RRR shoulder joints are labeled serially: j_1, j_2, and j_3.

variants of this configuration align j_1 slightly upwards and/or to the rear to optimize range of motion for a particular application [16]. A favorable aspect of this configuration is that when the upper arm is singular, twisting of the robot torso about the vertical axis will provide redundancy for the shoulder. However, in this configuration a spring counterbalance for the upper arm would require universal joints at either end, making the mechanical design quite complicated.

For all configurations, there is a constant struggle to package the counterweights or counterspring assemblies compactly. A counterweight mounted directly to the upper arm interferes severely with the torso during abduction, and with spring-based methods, interference between the arm and spring ground connection also reduces the range-of-motion.

III. DESIGN AND CONSTRUCTION

A. Differential Shoulder Design

Figure 3 illustrates the basic mechanics of joints j_1 and j_2 for configuration D. Coordinate frame C_0 is grounded; C_1 rotates with angle θ_1 about the $\mathbf{z}_0$-axis during arm flexion; C_2 is attached to the upper arm (before the arm rotation joint, j_3) undergoing flexion and abduction.

To ground the motors and counterbalance system, we first calculate gravity torques in the C_0-frame. Where R_i^j is the rotation matrix from the C_i to C_j frame, the location of the center of mass, m, as measured in C_0 is given by $\mathbf{r}_m^0 = R_1^0 R_2^1 \mathbf{r}_m^2$. The rotation matrices are calculated from the unit vectors, $R_i^j = e_a^i e_b^j$; following Figure 3, we find

$$\mathbf{r}_m^0 = \begin{bmatrix} \cos\theta_1 \sin\theta_2 & -\sin\theta_1 & -\cos\theta_1 \cos\theta_2 \\ \sin\theta_1 \sin\theta_2 & \cos\theta_1 & -\sin\theta_1 \cos\theta_2 \\ \cos\theta_2 & 0 & \sin\theta_2 \end{bmatrix} \mathbf{r}_m^2. \tag{7}$$

The center of mass of the upper arm is located a distance L from the shoulder, $\mathbf{r}_m^2 = L\mathbf{z}_2$. The vertical component of the center of mass in the rest frame is thus

$$\left(\mathbf{r}_m^0\right)_x = -L \cos\theta_1 \cos\theta_2. \tag{8}$$

To balance the arm, we need a counterbalance system with a potential energy that varies as $\cos\theta_1 \cos\theta_2$. A counterweight extending from the upper arm, as in figure 1-A, satisfies this requirement trivially. We can expand (8) using the product-to-sum identity,

$$\cos\theta_1 \cos\theta_2 = \frac{1}{2}\Big[\cos(\theta_1 + \theta_2) + \cos(\theta_1 - \theta_2)\Big]. \tag{9}$$

Notice that this equation has the form of a mechanical differential. Consider the configuration shown in Figure 4. The differential is represented as a pair of bevel gears in a one-sided cantilever configuration, rather than the balanced configuration of the WAM robot arm [3]. This configuration allows for continuous 360-degree flexion of the arm without interfering with the ground connection. In the rest position, counterbalance masses M_1 and M_2 stick up, at heights $\lambda_1 L$ and $\lambda_2 L$. The total potential energy of this system is

$$U = -mgL \cos\theta_1 \cos\theta_2$$
$$+ M_1 g \lambda_1 L \cos(\theta_1 + \theta_2) + M_2 g \lambda_2 L \cos(\theta_1 - \theta_2).$$

If we fix

$$M_1 L \lambda_1 = M_2 L \lambda_2 = \frac{1}{2} mL, \tag{10}$$

then we find $U = 0$ for all configurations, balancing the arm. A single counterweight has been split in two, each balancing half the arm's weight. During flexion the counterweights move in-phase, as if they were an extension of the arm. During abduction they move symmetrically out-of-phase, net center of mass dropping as the arm's center of mass rises.

A connecting hub, shown in blue, allows the counterweights to rotate continuously without interference; motors and counterbalances can be placed low in the torso,
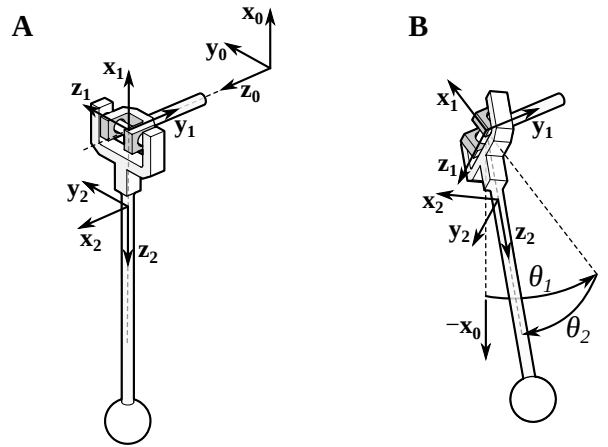

Fig. 3. (**A**) Coordinate frames shown in the reference position, upper arm hanging down. The base frame directions are superior (up): $\mathbf{x}_0$; posterior (back): $\mathbf{y}_0$; medial-to-lateral: $\mathbf{z}_0$. (**B**) Rotation of reference coordinate frames is shown for a superimposed flexion (θ_1) and abduction (θ_2) configuration.
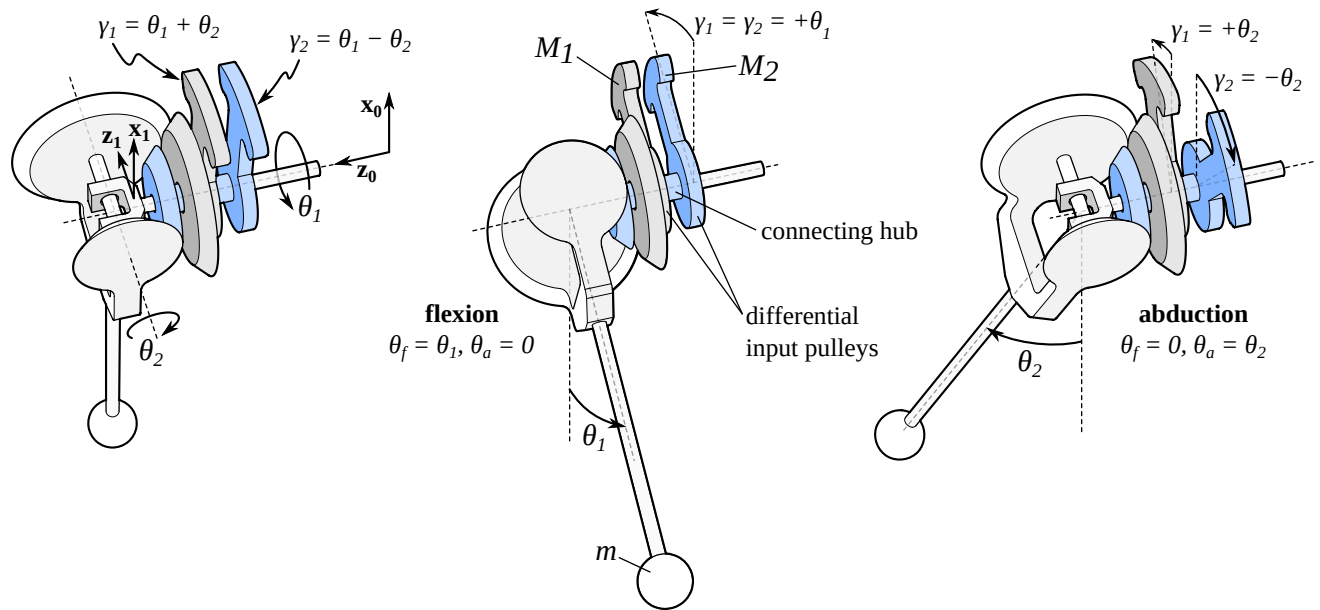
Fig. 4. (color) A differential is used to couple torques proportional to $(\theta_1 + \theta_2)$ and $(\theta_1 - \theta_2)$ to counterbalance the arm. For clarity, the differential is represented with bevel gears (teeth not shown). The two inputs of the differential are colored light blue and dark gray. The sense of flexion and abduction imply a frontal view of a right shoulder.

connected to the differential inputs by timing belts. The counterweights may be replaced with springs according to Figure 1-B. Even though the arm mass will increase by a factor of $(1 + 1/\lambda)$ when using a counterweight, much of this increase can be placed near the pelvis.

Note that the center of mass of the balanced system never moves in the $\mathbf{y}_0$-direction, which means that arm swing cannot be used to balance a walking robot in the sagittal plane. However, abduction of the arm does shift the center of mass laterally along the $\mathbf{z}_0$-axis, proportional to $\sin(\theta_2)$, which must be accounted for in the overall balancing of the robot.

B. Prototype Design

To explore this counterbalance design, we have produced a prototype arm, shown in Figure 5 and the accompanying video. The differential is achieved with cable capstans rather than bevel gears. Stock bevel gears come in a limited selection and cables offer advantages in stiffness, efficiency, and freedom from backlash. The cable differential is shown in Figure 6.

The output pulleys are split between their two capstan steps and a set-screw cable pre-tensioner is used. No grooves were machined into the capstans—with proper alignment and shimming, the capstans do not touch, and there is no tendency for the cables to slide off.

The counterweights are not attached to the shoulder input gears directly, as shown in Figure 4, but instead via a pair of 1:1 timing belts. This addition allows both the motors and the counterweights to be placed low in the body. Rubber-covered pinion wheels mounted to the motor shafts engage the counterbalance wheel rims in a friction drive, providing 12.5:1 and 10:1 torque amplification. The pinions

are elastically pre-loaded against the counterbalance wheel rims, so they are insensitive to moderate runout. Different diameter wheels are used so they may share a shaft.

C. Fabrication Methods

The cable differential, timing belt pulleys, and counterweight wheels are made from laminated laser-cut 4.5 mm acrylic. Dowel pins fit into post-laser reamed alignment holes to provide layer alignment. Bearing holes are post-drilled and ground for fit. The cable differential was found to require a capstan runout somewhat less than one-third to one-fourth of the cable diameter for braided nylon cord; we annealed each capstan acrylic layer against a flat reference surface in a temperature controlled oven to ensure flat, true-running capstans. Truing of the capstans on a lathe was not required.

The block inside the shoulder connecting the extension and abduction shafts is 3D printed, along with the motor mount straps. The u-shaped connector attaching the output pulleys, counterweight wheel friction rims, and the torso of the robot are laser-cut from 3 mm-thick birch plywood. These stacking and lamination-based prototyping methods are similar to and inspired by those shown in [17].

D. Operation and Performance

Compact hall-based absolute encoders are attached to each shaft at the shoulder joint and each motor is fitted with an optical encoder. The brushless motors are driven by off-the-shelf amplifiers. A Matlab xPC target computer runs the closed-loop controller at 1kHz using feedback from the joint encoders to calculate motor torques. Trajectory following in the accompanying video is achieved by rendering a simple spring and damper (PD control). This prototype was constructed to demonstrate the efficacy of the counterbalance
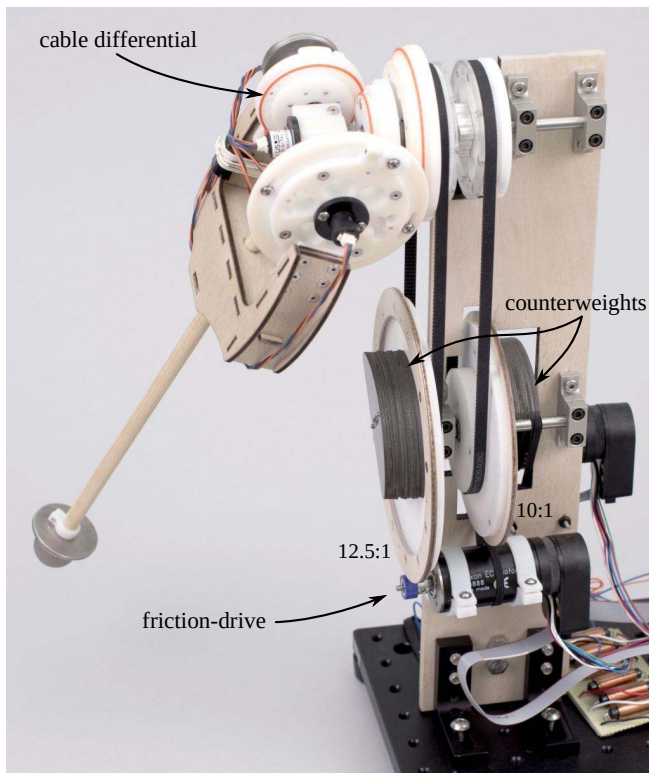
Fig. 5. (color) A complete view of the robot upper-arm, shoulder, and torso. Counterweights are stacks of water-jet cut steel plates attached to wood-rimmed wheels. These wheels are engaged by rubber-covered motor pinions. The two brushless motors are fitted with optical incremental encoders. Output angles are also measured at the shoulder with 10 bit absolute hall encoders.
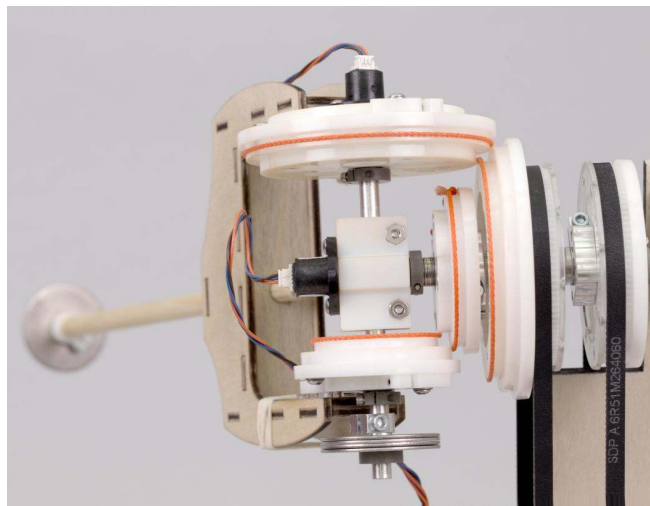

Fig. 6. (color) The cable differential is constructed from stacked laser-cut acrylic parts. The inner step of the small capstans is 40 mm in diameter. The cable is 1.5 mm braided nylon cord. The input pulleys attach to the motors and counterbalances below with 2 mm-pitch timing belts.

design and so tracking performance and payload capacity were not quantified.

The counterweights together weigh 456 grams and provide a maximum balancing torque of 0.13 N-m.

Because this prototype uses counterweights instead of springs and the counterbalance design is mathematically exact, the arm balances perfectly over the entire range-of-motion. All joints and pulleys in the robot use pre-loaded ball bearing pairs for minimum friction. To demonstrate that friction is not materially contributing to balancing, the motors were removed and the arm still balances perfectly, as shown in the video. Operation without counterweights and human interaction qualitatively demonstrate backdrivability.

A primary advantage of this design is the wide range of motion of the arm without interference between the counterbalance system and the robot body. Figure 7 illustrates the range of motion possible with this prototype. Theoretically, the range of motion could be almost a full sphere, limited only by interference with the body. A cable transmission cannot operate more than 360 degrees, less an allowance for cable termination. The prototype range of motion exceeds nominal human range-of-motion, excepting the usually-avoided singularity. This prototype can reach inward across the body up to 45 degrees for the entire

upper hemisphere of motion. Rotating the shoulder about the vertical axis allows placement of the singularity farther to the rear, without upsetting the counterbalance, at the expense of a reduced range of motion when reaching across the body. Previous counterbalance designs [1], [8], [9] are singular when the upper arm is vertical, restricting the range of motion to the extent that avoidance of the singular region is desirable. These spring-based methods also restrict motion above the head since the arm interferes with the ground connection of the balance spring located directly above the shoulder center of rotation.

IV. CONCLUSIONS AND FUTURE WORK

We have introduced a new method of counterbalancing robot arms. By the application of a differential, the upper arm mass and lumped mass of any lower arm is balanced perfectly over the complete range of motion. Since the split-counterbalances or counter-springs are remote to the shoulder, this method of counterbalancing does not restrict the range of motion of the arm beyond existing geometrical contraints on the range of motion. If a differential is already under consideration for the advantages of a parallel shoulder mechanism, then this particular arrangement allows for perfect gravity balancing with little added complexity.

Applications for this design fall into three areas. The first is robot arms that must be passively and utterly human safe, but also light and expressive. Entertainment and therapy robots are a natural fit here. The second area is when a robot arm must be absolutely counterbalanced for safety purposes and requires a large range of motion. For example, a robot performing a sensitive medical or surgical operation. To be both backdrivable and power-failure-safe, the robot must be counterbalanced, and this design might be appropriate if a large range of motion is also required or if the configuration
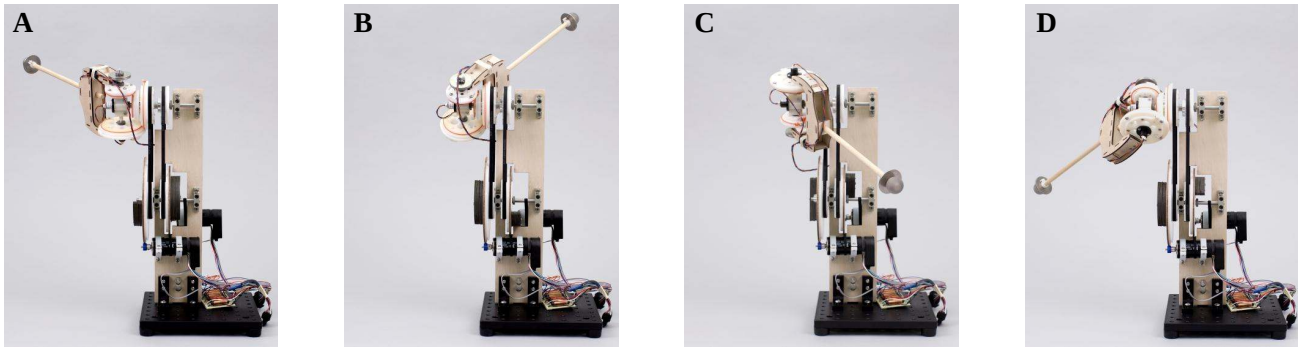
Fig. 7. (color) The range-of-motion of this upper-arm equals the human range-of-motion, and in some cases, such as view B, where the arm reaches back and medially, exceeds the normal human range. Interference when reaching across the body (B and C) is determined by interference between the arm and either the timing belts or the large capstans.

matching the motion of a human operator is desired. The third application is mobile robots where power consumption and range-of-motion are both critically important. Counterbalancing allows the motors to be sized for instantaneous torque ratings, and static power consumption is eliminated without sacrificing backdrivability. Wheeled mobile robots with dexterous arms are particularly suitable.

Arm rotation at the shoulder and elbow flexion are under active development. To remotely actuate these joints we are investigating fluid-based and other flexible transmission concepts. Alternatively, motors may be placed in the arm directly, which for this design fortunately does not require any increase is the static torque rating of the shoulder motors. To counterbalance the forearm, we will employ a simple pantograph as shown in Figure 1-C to move the forearm counterweight close to the shoulder, greatly reducing arm inertia. It is probable that the main counterweights will be replaced with zero free-length springs or cable-spring assemblies [13] to reduce torso weight further. Each spring operates in a single plane, simplifying their mounting and integration. Each input pulley has unrestricted 360-degree continuous rotation, which allows compact and interference-free mounting of counterbalance springs.

ACKNOWLEDGMENT

REFERENCES

[1] K. A. Wyrobek, E. H. Berger, H. M. Van der Loos, and J. K. Salisbury, "Towards a personal robotics development platform: Rationale and design of an intrinsically safe personal robot," in *Proc. IEEE International Conference on Robotics & Automation (ICRA'08)*, 2008, pp. 2165–2170.

[2] C.-H. King, T. L. Chen, A. Jain, and C. C. Kemp, "Towards an assistive robot that autonomously performs bed baths for patient hygiene," in *Proc. IEEE International Conference on Intelligent Robots and Systems (IROS'10)*, 2010, pp. 319–324.

[3] K. Salisbury, W. Townsend, B. Ebrman, and D. DiPietro, "Preliminary design of a whole-arm manipulation system (wams)," in *Proc. IEEE International Conference on Robotics and Automation, (ICRA'98)*, 1988, pp. 254–260.

[4] A. J. Madhani, G. Niemeyer, and J. K. Salisbury Jr, "The Black Falcon: A teleoperated surgical instrument for minimally invasive surgery," in *Proc. IEEE International Conference on Intelligent Robots and Systems*, vol. 2, 1998, pp. 936–944.

[5] W. Knight, "This robot could transform manufacturing," *MIT Technology Review*, September 2012.

[6] M. Zinn, O. Khatib, B. Roth, and J. K. Salisbury, "Playing it safe," *IEEE Robotics and Automation Magazine*, vol. 11, no. 2, pp. 12–21, 2004.

[7] N. Hogan and S. P. Buerger, "Impedance and interaction control," in *Robotics and automation handbook*. CRC Press, 2005, pp. 19–1–19–24.

[8] G. J. Tuijthof and J. L. Herder, "Design, actuation and control of an anthropomorphic robot arm," *Mechanism and machine theory*, vol. 35, no. 7, pp. 945–962, 2000.

[9] M. Vermeulen and M. Wisse, "Intrinsically safe robot arm: Adjustable static balancing and low power actuation," *International Journal of Social Robotics*, vol. 2, no. 3, pp. 275–288, 2010.

[10] T. Rahman, W. Sample, S. Jayakumar, M. M. King, J. Y. Wee, R. Seliktar, M. Alexander, M. Scavina, and A. Clark, "Passive exoskeletons for assisting limb movement," *Journal of rehabilitation research and development*, vol. 43, no. 5, pp. 583–589, 2006.

[11] C. Cho, W. Lee, and S. Kang, "Static balancing of a manipulator with hemispherical work space," in *Proc. IEEE/ASME International Conference on Advanced Intelligent Mechatronics (AIM'10)*, 2010, pp. 1269–1274.

[12] M.-A. Lacasse, G. Lachance, J. Boisclair, J. Ouellet, and C. Gosselin, "On the design of a statically balanced serial robot using remote counterweights," in *Proc. IEEE International Conference on Robotics & Automation (ICRA'13)*, 2013, pp. 4174–4179.

[13] J. L. Herder, "Energy-free systems: theory, conception, and design of statically balanced spring mechanisms," Ph.D. dissertation, Delft University of Technology, 2001.

[14] I. A. Kapandji, *The Physiology of the Joints. Volume 1: The Upper Limb*. Churchill Livingstone, 1987.

[15] J. Kober, M. Glisson, and M. Mistry, "Playing catch and juggling with a humanoid robot," in *Proc. IEEE-RAS International Conference on Humanoid Robots*, 2012.

[16] N. S. Pollard, J. K. Hodgins, M. J. Riley, and C. G. Atkeson, "Adapting human motion for the control of a humanoid robot," in *Proc. IEEE International Conference on Robotics and Automation, (ICRA'02)*, vol. 2, 2002, pp. 1390–1397.

[17] M. Quigley, A. Asbeck, and A. Ng, "A low-cost compliant 7-DOF robotic manipulator," in *Proc. IEEE International Conference on Robotics and Automation, (ICRA'11)*, 2011, pp. 6051–6058.